Open-porous Silicon Nitride-based Ceramics in Tubular Geometry Obtained by Slip-casting and Gelcasting **

By *Dominik Brouczek*, and *Thomas Konegger**

[*] *Dr. Thomas Konegger, Dominik Brouczek*
TU Wien, Institute of Chemical Technologies and Analytics
Getreidemarkt 9/164-CT, 1060 Vienna, Austria
E-mail: thomas.konegger@tuwien.ac.at

[**] *The authors thank T. Prochaska for his assistance in porosimetry and XRD measurements. Partial support of this study by the Austrian Science Fund (FWF): P 29058-N34 is gratefully acknowledged. Supporting Information is available online from Wiley InterScience or from the author.*

Owing to its unique properties, silicon nitride is a frequently used materials choice in highly demanding applications in terms of thermal and mechanical load. In this work, porous silicon nitride-based support materials in hollow-tube configuration are generated through colloidal forming, and their respective properties for potential applications in the fields of membrane-based separation, filtration, or catalysis are evaluated. Shaping of the ceramics is achieved by two distinct casting techniques, slip-casting and gelcasting, and the results of the respective methods are set in relation. Furthermore, a special focus is set on the correlation between sintering parameters and resulting porosity. Subsequently, air permeabilities of the generated structures are determined, illustrating a direct relation between processing parameters and resulting permeability. Darcian permeability values of up to $9 \cdot 10^{-16}$ m^2 *are observed for samples exhibiting total porosities between 32 % and 41 %. The findings allow*

for a predictability of suitable permeation properties for the structures' anticipated application as complex-shaped non-oxide ceramic supports for membrane-based separation or catalysis, or as high-performance filter materials.

1. Introduction

Silicon nitride (Si_3N_4), a non-oxide ceramic, is widely used as structural material owing to its outstanding properties, including high mechanical strength, high thermal and chemical stability, as well as its resistance to oxidation and corrosion.[1, 2] As opposed to the traditional aim towards achieving full densification of ceramics during consolidation in order to achieve high structural integrity, the advantages of Si_3N_4 with well-defined porosity have lately been exploited for various applications in the fields of filtration, catalysis, or in membrane technology.[3, 4] Separation processes employing porous ceramic materials, such as micro- and ultrafiltration or gas separation, have gained increasing attention in various industrial sectors, reaching from chemical and biochemical processing to energy- and environment-related fields, with the particular benefit of improved operability in harsh thermal and chemical environments compared to conventional polymer-based materials.[5]

A wide variety of methods and approaches has been reported on the generation of porous Si_3N_4 and related ceramics, including direct foaming,[6] the addition of pore-forming agents,[7-9] combustion synthesis,[10] freeze-casting,[11] or phase separation.[12] Another straightforward approach is partial sintering, where the sintering process is halted before full densification, thus retaining an open-porous pore network between partially connected Si_3N_4 particles in the final material.[13] A distinct advantage of this approach is the possibility to combine it with colloidal processing strategies such as slip-casting[14] or gelcasting.[15, 16] These techniques allow for the fabrication of complex-shaped structures, an important requirement for potential applicability: in most previous reports on porous Si_3N_4 ceramics, only simple geometries were obtained, thus limiting the applicability due to a decreased functional surface. Generally, for

prospective applications as support material for membranes or catalysts, a tubular configuration is preferred, resulting in an increased surface-to-volume ratio compared to planar setups.[5, 17]

The objective of this work is the implementation of two distinct colloidal processing strategies – slip-casting and gelcasting – in combination with partial sintering for generating porous Si_3N_4 ceramics in tubular configuration. Properties relevant for their prospective use as support structures, including porosity, pore size, and permeability of porous Si_3N_4 specimens, are evaluated with respect to sintering temperature and processing route chosen in order to gain insights on the selection of adequate preparation conditions to achieve desired combinations of pore morphology and permeating flux.

2. Experimental Procedure

Tubular specimens consisting of particulate Si_3N_4 with sintering aids were produced following two distinct colloidal processing routes, slip-casting and gelcasting. In both cases, partial sintering was carried out in the temperature range between 1500 to 1600 °C before characterization of material properties.

2.1. Preparation of slip-cast specimens

Si_3N_4 powder (*SN-E10, UBE Industries,* $d_{50} \approx 0.7$ µm, α-phase content > 95 wt.%) and deionized water were used to prepare an aqueous slurry of 36 vol.% solid content (62 wt.% Si_3N_4), including 2.5 wt.% Al_2O_3 (*CT3000 SG, Almatis,* $d_{50} \approx 0.5$ *µm)* and 2.5 wt.% Y_2O_3 (*Grade C, H.C. Starck,* $d_{50} \approx 0.8$ *µm),* with respect to Si_3N_4, as sintering aids. An amino alcohol-based dispersing agent (*Dolapix A88, Zschimmer und Schwarz*) was added (0.6 wt.% with respect to Si_3N_4). The resulting aqueous slurry of Si_3N_4 powder and sintering aids was fully homogenized by ball-milling for 24 h using Si_3N_4 balls.

Subsequently, the de-aired flowable mixture was cast into two-part plaster molds made of a formulated hemihydrate plaster (*Supraduro)*, where it remained for 70 s. During this time, ceramic particles of the slurry were deposited on the plaster surface, forming tubular specimens. Subsequently, the excess slurry was removed. After a drying period, green bodies with outer diameters of 12 mm, lengths of up to 60 mm, and an average wall thickness of 1.8 mm were demolded and dried at 110 °C in a drying cabinet.

Consolidation of the porous tubular Si_3N_4 structures was achieved by partial sintering in a high-temperature graphite furnace for 2 hours in high-purity nitrogen atmosphere (0.1 MPa) at temperatures of 1500, 1550 and 1600° C, respectively, using a heating rate of 10 K min^{-1}. To suppress decomposition of the Si_3N_4 compound, samples were sintered in a powder bed consisting of Si_3N_4 and BN (50 wt.% each).

2.2. Preparation of gelcast specimens

For the gelcasting process, gelling agents were added to an aqueous silicon nitride slurry. Methacrylamide (*MAM*, *Sigma-Aldrich*) was used as monomer, N,N‘-Methylenebisacrylamide (*MBAM, Sigma-Aldrich*) as crosslinker, and ammonium persulfate (*APS*, Sigma-Aldrich) as initiator for this gelling system.

Based on work by Janney *et al.*,[18] a 15 wt.% monomer solution in deionized water was prepared having an MAM to MBAM weight ratio of 6:1. Corresponding amounts of Si_3N_4 powder and the sintering aids (2.5 wt.% Al_2O_3 and 2.5 wt.% Y_2O_3 with respect to Si_3N_4) were then added and a slurry with a solid loading of 45 vol.% (69 wt.% Si_3N_4) was obtained. In this route, 5 wt.% of dispersant with respect to Si_3N_4 (*Dolapix A88, Zschimmer und Schwarz*) were added. The mixture was fully homogenized by ball-milling for 72 h followed by degassing.

Subsequently, a 10 wt.% aqueous APS solution (volume ratio of Si_3N_4 slurry to 10 wt.% APS of 93:1) was added to the mixture, starting the gelation. After two minutes of homogenization,

the flowable slurry was immediately cast into molds defining the tubular shape, consisting of a two-part elastomeric cup made of a condensation-curing polydimethylsiloxane compound (*MoldMax XLS II, Smooth-On Inc.*). The elastomeric molds were preconditioned at 110 °C before casting to remove any residual moisture. In the center of the elastomeric cup, a paraffin wax rod was positioned and held in place by a cavity and an aluminium lid with a corresponding bore.

After two days at 40 °C in the drying cabinet, the fully cured specimens were demolded. The paraffin wax core was removed by melting at 58 °C for 1 h in the drying cabinet, followed by final drying of the samples at 110 °C. Green bodies with outer and inner diameters of 12 and 8 mm, respectively, and lengths of up to 43 mm were obtained.

Debinding was conducted in flowing N_2 (0.5 L min^{-1}) for 1 h at 700 °C in a tube furnace, using a heating rate of 1 K min^{-1}. Finally, debinded specimens were partially sintered in analogy to the slip-cast samples.

2.3. Characterization

Density and apparent porosity of sintered specimens were determined by the water immersion method, following EN 623-2.[19] Microstructural features were illustrated by scanning electron microscopy (Quanta 200, FEI, Netherlands). Mercury intrusion porosimetry was used for determination of pore size distributions (Pascal 140/440, Porotec GmbH, Germany).

Gas permeability experiments were carried out at room temperature using filtered compressed air as fluid. Tubular specimens with an outer diameter of 10 to 11 mm, a wall thickness of around 1.5 to 2 mm, and a length between 30 and 40 mm were positioned in a test rig and sealed with rubber O-rings. The stationary permeating gas flow Q through the tube walls was recorded as a function of the pressure drop Δp between upstream (p_i) and downstream (p_0) side of the specimen. The permeated area A and wall thickness l were calculated from the sample dimensions. A minimum of 3 specimens were tested for each parameter combination.

For slip-cast samples, a minimum of five sets of Δp and Q were recorded per sample, varying Δp between 0.2 and 1 bar. For gelcast samples, nine sets of Δp and Q were recorded, up to maximum Δp values of 3 bar. Permeability coefficients (both Darcian, k_1, and Non-Darcian, k_2) were determined using Forchheimer's equation for compressible fluids, employing a quadratic fit to $(p_i^2-p_0^2)/(2p_0 \cdot l)$ using the least-squares method[20] (assuming an air viscosity η of $1.84 \cdot 10^{-5}$ Pa·s and an air density ρ of 1.15 kg·m^{-3}), equation 1:

$$\frac{p_i^{\,2} - p_o^{\,2}}{2 p_0 \cdot l} = \frac{\eta}{k_1}\frac{Q}{A} + \frac{\rho}{k_2}\left(\frac{Q}{A}\right)^2 \qquad (1)$$

3. Results and Discussion

3.1. Sample preparation and consolidation

Slip-casting was found to be a straightforward method for the preparation of tubular specimens with well-defined geometries. After preliminary investigations to determine the rate of slip deposition for the slurry used, tubular specimens with outer diameters of 12 mm, wall thicknesses of 1.8 mm, and lengths of up to 60 mm were formed. Maintaining the determined time schedule for demolding and drying facilitated the reproducible preparation of crack-free green specimens. Even without addition of binder compounds, green strength was sufficient for sample handling. Subsequently, sintering in nitrogen atmosphere in a protective powder bed resulted in crack-free tubular final structures, without observing decomposition of the Si_3N_4 compound (**Figure 1**).

In contrast to the slip-casting process, where close packing of colloidal particles is achieved through the removal of water by the plaster mold, no such driving force is present in gelcasting. As a consequence, significantly higher solid loadings were needed to form slurries suitable for gelcasting, requiring a higher concentration of dispersant and longer times of slurry homogenization. By modifying the slurry composition and employing a well-defined gelling/drying regime, compact, crack-free green bodies were successfully formed. After a

debinding treatment in inert atmosphere, samples were transferred to a separate furnace for the sintering treatment. The final specimens showed no visible residues from the organic binder system (**Figure 1**).

Depending on the sintering temperature, linear shrinkage rates in the range of 7 to 11 % were observed for both slip- and gelcast samples.

3.2. Microstructure and porosity

The colloidal processing procedures resulted in slurries with high stability, facilitating the generation of microstructures without the presence of large-scale particle agglomerations (**Figure 2**). By limiting the sintering temperature to 1600 °C, only partial sintering occurred between Si_3N_4 particles. As a result, a continuous, open pore structure was maintained in the material while achieving adequate mechanical strength through neck formation between particles. In the sintering temperature range observed, Si_3N_4 grains retained their equiaxed shape. X-ray diffraction analysis showed some transformation of α-Si_3N_4 to β-Si_3N_4 (diffractograms can be found in the supporting information), however, no formation of rod-like β-Si_3N_4 grains was observed.

Variation of the sintering temperature between 1500 °C and 1600 °C resulted in open porosities between 32 and 41 % for both slip-cast and gelcast samples (**Table 1**), thus coinciding with the target porosity range of 30 to 40 %, a porosity range typically chosen, e.g., for membrane support structures. As expected, an increase in sintering temperature led to a well-defined decrease in total porosity due to advancing sintering processes between Si_3N_4 particles.

Sintering temperature was found to also affect pore size in the temperature range investigated (**Figure 3**). A slight shift of the pore size towards higher values was found for increased sintering temperatures, e.g. increasing from median pore opening diameters of 0.16 µm and 0.18 µm at 1500 °C to 0.18 µm and 0.23 µm at 1600 °C for slip-cast and gelcast samples,

respectively (**Table 1**). This temperature-dependent size shift can be explained as a result of pore window widening by sintering-caused rounding of interparticle voids.[21] It can be expected that to some extent, further increase of the pore opening diameter is possible through increased sintering temperatures, with a simultaneous decrease in total porosity. Slightly higher total porosity and larger pore opening diameters were found in gelcast specimens. Possible explanations are a lower degree of particle packing during green consolidation when compared to slip-casting, in addition to voids resulting from the removal of organic compounds present in the starting mixture. Furthermore, partial hydrolysis or oxidation of the Si_3N_4 particles as a result of the longer exposure to water and oxidizing agents during the gelcasting procedure may result in the formation of additional secondary – primarily oxidic – phases, which in turn may affect the sintering process and cause the slight differences in the sintering behavior between slip-cast and gelcast Si_3N_4 particles.

3.3. Permeability characteristics

For the prospective applications of the materials generated, evaluation of permeability characteristics is of major importance. As such, all samples generated were tested in terms of air permeability, recording permeating flows at given pressure drops (**Figure 4**). Pairs of permeating flow and pressure drop were fitted to the relation by Forchheimer (Eq.1), yielding the respective Darcian (k_1) and Non-Darcian (k_2) permeability constants for slip-cast and gelcast specimens (**Figure 5**). In all samples, both viscous and inertial contributions to overall permeability were observed. The Darcian permeability constants k_1 reached values between 10^{-16} and 10^{-15} m^2, the highest values observed for samples sintered at 1500 °C. Non-Darcian permeabilities k_2 varied between 10^{-11} and 10^{-10} m.

As no pronounced change in pore opening diameter was observed in the processing parameter range chosen, permeabilities could be directly correlated to the total porosities of individual specimens (**Figure 6**). In accordance with slightly higher total porosities and pore opening

diameters of gelcast materials, increased permeabilities were observed for samples generated through this processing technique.

The observed upper limit of 10^{-15} m^2 for Darcian permeability is a direct result of the use of a fine starting powder (d_{50} around 0.7 µm), as well as the use of colloidal processing techniques, leading to a rather dense packing of particles in green state compared to other forming techniques such as powder pressing. However, benefits of this route include the significant reduction in the number of large defects, including agglomerates and voids, in the final structure. Further improvements of the permeability without increasing total porosity and hence reducing mechanical integrity, e.g. by an increase in pore opening diameter, are generally possible by using coarser starting powders; on the downside, this detrimentally affects the resulting surface quality, an important factor e.g. in membrane technology. Attempts to achieve this compromise by modifying other process parameters such as particle shape are currently underway.

4. Conclusions

In this work, we demonstrated two casting-based approaches to generate open-porous silicon nitride-based structures in tubular geometry, with the goal to generate porous non-oxide ceramic materials suitable for application in the fields of membrane-based separation, catalysis, or filtration. We showed that comparable pore structures and, as a result, comparable permeability characteristics could be achieved through both conventional slip-casting as well as gelcasting. While the first method was shown to be highly suitable for the straightforward generation of tubular structures, e.g., as support structures for membranes or catalysts, the latter method allows for an even higher flexibility in terms of geometries obtainable, thus facilitating the generation of materials for prospective applications with particular shape requirements such as complex-shaped filters.

Resulting from the use of a fine silicon nitride starting powder and targeted maximum porosities of 40 %, maximum permeabilities in the range of 10^{-15} m^2 were observed. For applications requiring higher fluid throughputs, further tailoring of the pore structure (e.g., an increase in opening pore diameter) in order to achieve higher permeability values is possible by variation of starting materials or sintering parameters; further work in this direction is currently in progress.

References:

[1] F. L. Riley, *J. Am. Ceram. Soc.* **2000**, *83*, 245.

[2] H. Klemm, *J. Am. Ceram. Soc.* **2010**, *93*, 1501.

[3] T. Ohji, M. Fukushima, *Int. Mater. Rev.* **2012**, *57*, 115.

[4] M. Scheffler, P. Colombo, in *Cellular Ceramics*, Wiley-VCH Verlag, Weinheim **2005**.

[5] K. Li, in *Ceramic Membranes for Separation and Reaction*, Wiley, Chichester **2007**.

[6] J. Yu, J. Yang, H. Li, Y. Huang, *J. Porous Mater.* **2012**, *19*, 883.

[7] F. Chen, Q. Shen, F. Yan, L. Zhang, *J. Am. Ceram. Soc.* **2007**, *90*, 2379.

[8] T. Konegger, R. Patidar, R. K. Bordia, *J. Eur. Ceram. Soc.* **2015**, *35*, 2679.

[9] T. Konegger, L. F. Williams, R. K. Bordia, *J. Am. Ceram. Soc.* **2015**, *98*, 3047.

[10] D. Chen, B. Zhang, H. Zhuang, W. Li, *Ceram. Int.* **2003**, *29*, 363.

[11] T. Fukasawa, Z.-Y. Deng, M. Ando, T. Ohji, S. Kanzaki, *J. Am. Ceram. Soc.* **2002**, *85*, 2151.

[12] J. Yue, B. Dong, H. Wang, *J. Am. Ceram. Soc.* **2011**, *94*, 1989.

[13] A. Kalemtas, G. Topates, H. Özcoban, H. Mandal, F. Kara, R. Janssen, *J. Eur. Ceram. Soc.* **2013**, *33*, 1507.

[14] H. Mori, S. Mase, N. Yoshimura, T. Hotta, K. Ayama, J. I. Tsubaki, *J. Membr. Sci.* **1998**, *147*, 23.

[15] J. Yu, H. Wang, J. Zhang, D. Zhang, Y. Yan, *J. Sol-Gel Sci. Technol.* **2010**, *53*, 515.

[16] T. Wan, D. Yao, H. Hu, Y. Xia, K. Zuo, Y. Zeng, *Mater. Lett.* **2014**, *133*, 190.

[17] T. Konegger, T. Prochaska, R. Obmann, *J. Ceram. Soc. Jpn.* **2016**, *124*, 1030.

[18] M. A. Janney, O. O. Omatete, C. A. Walls, S. D. Nunn, R. J. Ogle, G. Westmoreland, *J. Am. Ceram. Soc.* **1998**, *81*, 581.

[19] European Standard EN 623, Advanced technical ceramics; Monolithic ceramics – general and textural properties; Part 2: Determination of density and porosity: EN 623-2 (1993)

[20] M. Innocentini, P. Sepulveda, F. Ortega, in *Cellular Ceramics* (Eds: M. Scheffler, P. Colombo), Wiley-VCH **2005**, 313.

[21] A. Akash, M. J. Mayo, *J. Am. Ceram. Soc.* **1999**, *82*, 2948.

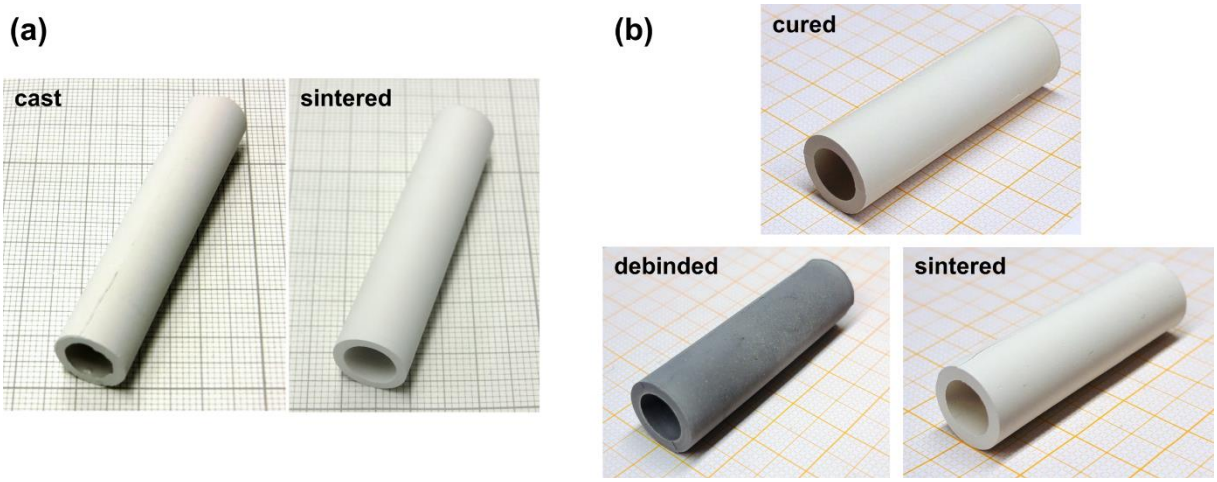

Fig. 1. Morphology and appearance of (a) slip-cast and (b) gelcast silicon nitride specimens during various processing stages

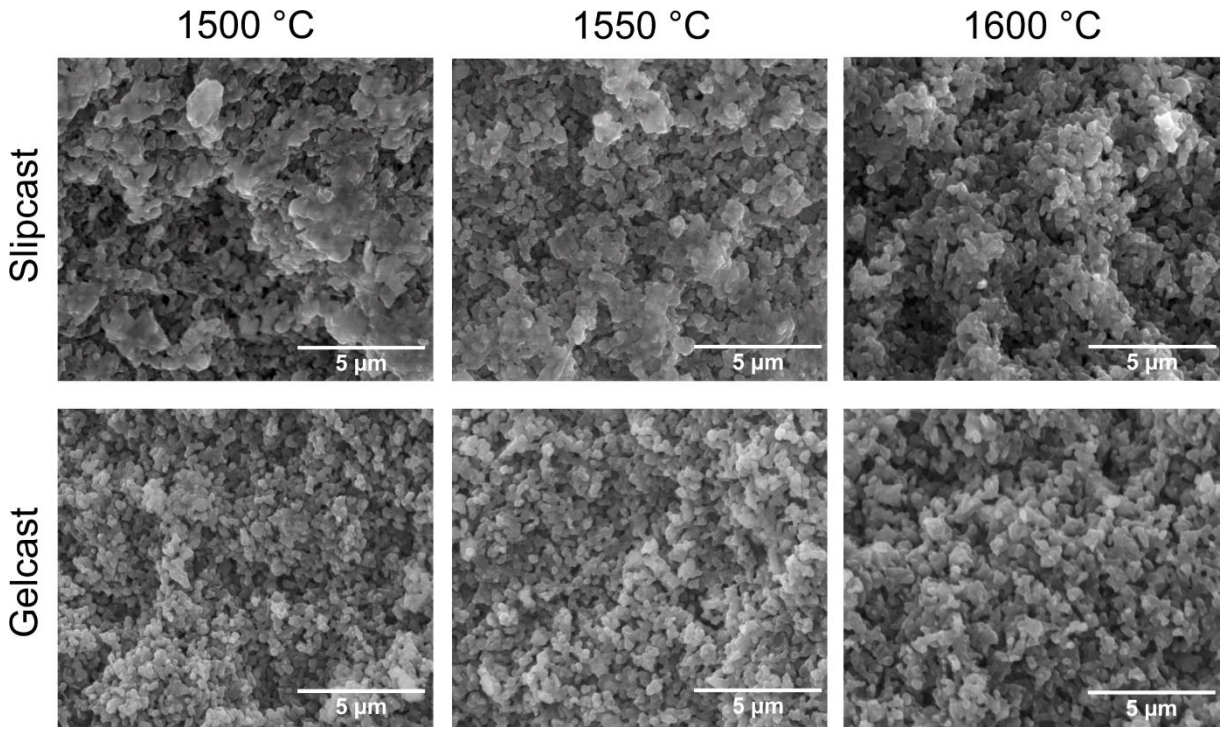

Fig. 2. Fracture surfaces of slip-cast (top) and gelcast samples (bottom), after sintering at various temperatures

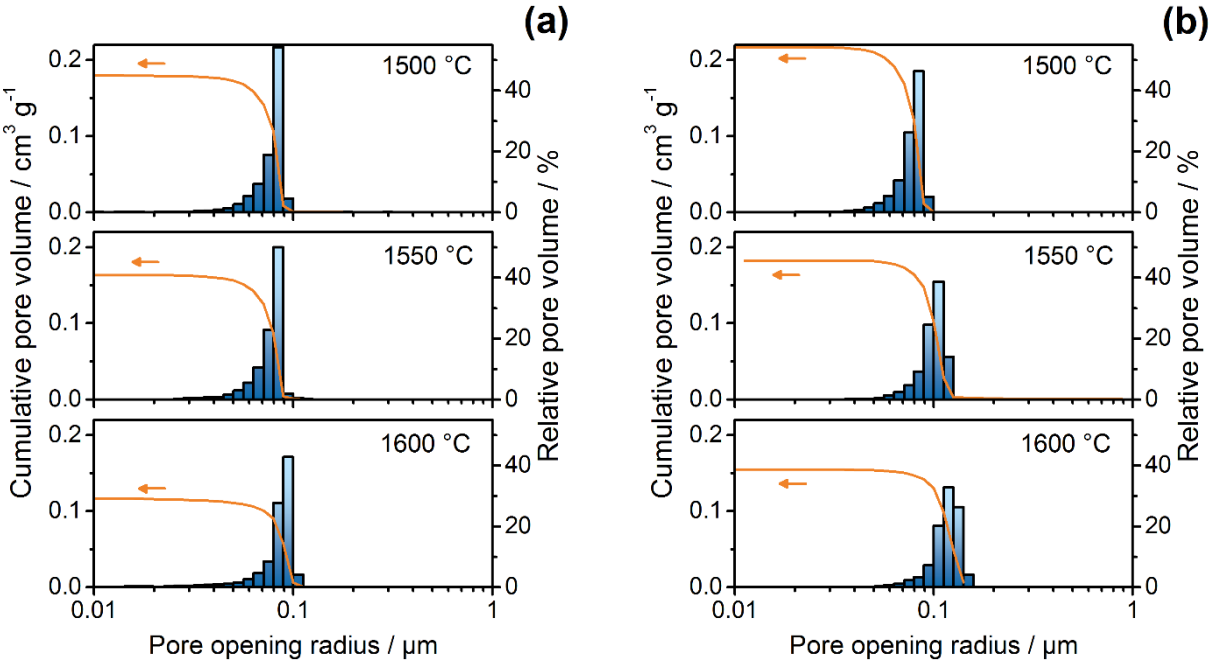

Fig. 3. Pore opening radius distribution of (a) slip-cast and (b) gelcast samples as function of sintering temperature (determined by Hg porosimetry)

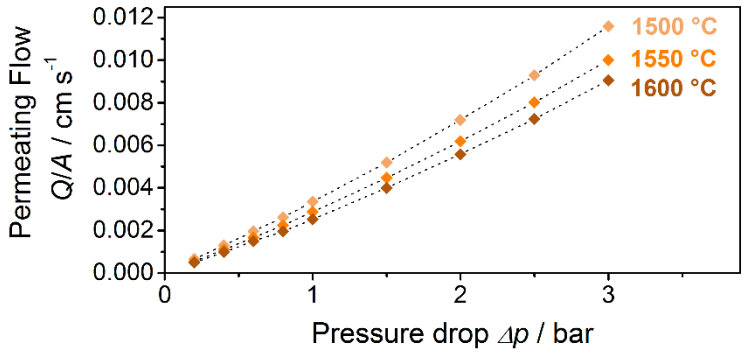

Fig. 4. Typical gas flow curves of samples sintered at different temperatures (exemplary for gelcast materials)

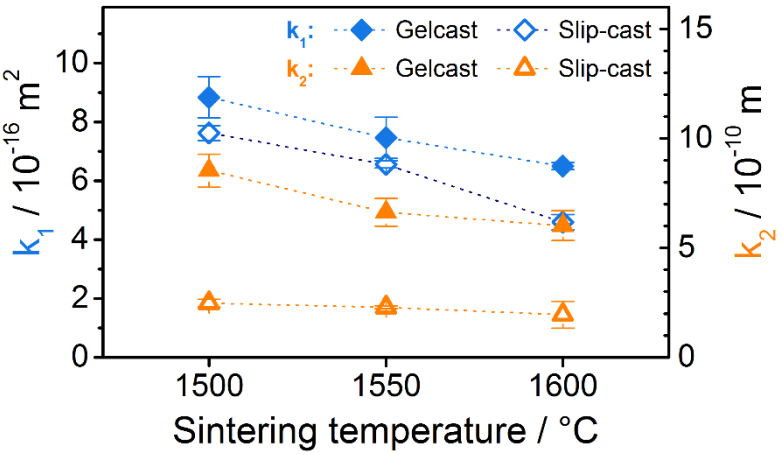

Fig. 5. Effect of sintering temperature on Darcian (k_1) and Non-Darcian (k_2) permeabilities of slip-cast and gelcast samples

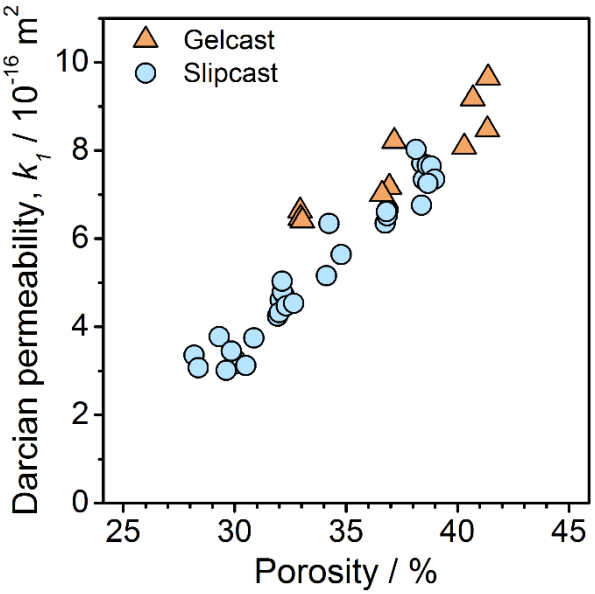

Fig. 6. Correlation between air permeability and porosity of slip-cast and gelcast samples

Table 1. Total porosity (determined by water immersion method) and median pore opening diameter (determined by Hg porosimetry) of sintered slip-cast and gelcast specimens

Sintering temperature [°C]	Porosity (slip-cast) [%]	Median pore opening diameter (slip-cast) [µm]	Porosity (gelcast) [%]	Median pore opening diameter (gelcast) [µm]
1500	38.6 ± 0.3	0.16	40.9 ± 0.5	0.18
1550	36.8 ± 0.2	0.16	36.9 ± 0.3	0.20
1600	32.3 ± 0.3	0.18	33.0 ± 0.1	0.23